2012

Long-range correlations in Fourier transform infrared, satellite, and modeled CO in the Southern Hemisphere

Olaf Morgenstern
National Institute of Water and Atmospheric Research, New Zealand

Guang Zeng
National Institute of Water and Atmospheric Research, New Zealand

Stephen W. Wood
Formerly at National Institute of Water and Atmospheric Research, New Zealand

John Robinson
National Institute of Water and Atmospheric Research, New Zealand

Dan Smale
National Institute of Water and Atmospheric Research, New Zealand

See next page for additional authors

Long-range correlations in Fourier transform infrared, satellite, and modeled CO in the Southern Hemisphere

Abstract

We use Fourier transfonn infrared ground-based measurements and satellite and model data to assess long-range correlations in tropospheric carbon monoxide. We fmd that CO columns measured in New Zealand correlate well with those measured in Antarctica, if a transport-related lag is taken into account. The model suggests that this long-range correlation is part of a mode of anomalous CO comprising almost the whole southern extratropics, which is linked to biomass burning in the southern continents. No such mode is modeled for the Northern Hemisphere. The area of long-range correlations maximizes for the southern subtropical Pacific, which is identified as an advantageous location for a hypothetical new measurement station. The satellite data (produced by the Measurements of Pollution in the Troposphere (MOPITT) instrument) partially confinn these fmdings but with generally reduced correlations. In particular, the satellite data suggest no long-range correlation at high latitudes. This is partially explained in terms of retrieval limitations and partially reflects a model deficiency.

Keywords

fourier, infrared, transform, modeled, correlations, satellite, range, long, co, southern, hemisphere, GeoQUEST

Disciplines

Life Sciences | Physical Sciences and Mathematics | Social and Behavioral Sciences

Publication Details

Morgenstern, O., Zeng, G., Wood, S. W., Robinson, J., Smale, D., Paton-Walsh, C., Jones, N. B. & Griffith, D. W. T. (2012). Long-range correlations in Fourier transform infrared, satellite, and modeled CO in the Southern Hemisphere. Journal of Geophysical Research D: Atmospheres, 117 (11), D11301.

Authors

Olaf Morgenstern, Guang Zeng, Stephen W. Wood, John Robinson, Dan Smale, Clare Paton-Walsh, Nicholas B. Jones, and David W. T Griffith

Long-range correlations in Fourier transform infrared, satellite, and modeled CO in the Southern Hemisphere

Olaf Morgenstern,[1] Guang Zeng,[1] Stephen W. Wood,[2] John Robinson,[1] Dan Smale,[1] Clare Paton-Walsh,[3] Nicholas B. Jones,[3] and David W. T. Griffith[3]

Received 16 February 2012; revised 18 April 2012; accepted 18 April 2012; published 1 June 2012.

[1] We use Fourier transform infrared ground-based measurements and satellite and model data to assess long-range correlations in tropospheric carbon monoxide. We find that CO columns measured in New Zealand correlate well with those measured in Antarctica, if a transport-related lag is taken into account. The model suggests that this long-range correlation is part of a mode of anomalous CO comprising almost the whole southern extratropics, which is linked to biomass burning in the southern continents. No such mode is modeled for the Northern Hemisphere. The area of long-range correlations maximizes for the southern subtropical Pacific, which is identified as an advantageous location for a hypothetical new measurement station. The satellite data (produced by the Measurements of Pollution in the Troposphere (MOPITT) instrument) partially confirm these findings but with generally reduced correlations. In particular, the satellite data suggest no long-range correlation at high latitudes. This is partially explained in terms of retrieval limitations and partially reflects a model deficiency.

Citation: Morgenstern, O., G. Zeng, S. W. Wood, J. Robinson, D. Smale, C. Paton-Walsh, N. B. Jones, and D. W. T. Griffith (2012), Long-range correlations in Fourier transform infrared, satellite, and modeled CO in the Southern Hemisphere, *J. Geophys. Res.*, *117*, D11301, doi:10.1029/2012JD017639.

1. Introduction

[2] The Network for the Detection of Atmospheric Composition Change (NDACC) maintains a substantial number of stations dedicated to ground-based observations of atmospheric composition (http://www.ndsc.ncep.noaa.gov). It has been instrumental in recording baselines, trends, and variability of constituents of both tropospheric and stratospheric interest. In the troposphere, causes for interannual variability include biomass burning events [e.g., *Crutzen et al.*, 1979; *Crutzen and Carmichael*, 1993; *Jones et al.*, 2001; *Edwards et al.*, 2006a; *Yashiro et al.*, 2009] and meteorological events such as El Niño [*Rinsland et al.*, 1999; *Zhang*, 2011; *Edwards et al.*, 2006b]. NDACC comprises 18 stations that operate or have operated Fourier transform infrared (FTIR) spectrometers [*Rinsland et al.*, 1998] used to infer a large variety of species. Two of them, Lauder (45°S, 170°E) and Wollongong (34°S, 151°E), are located in southern midlatitudes, and only one, Arrival Heights (78°S, 167°E), is located in Antarctica. This means that southern middle and high latitudes are extremely sparsely sampled by FTIR.

[3] *Chatfield et al.* [2002] describe a plume of elevated carbon monoxide (CO) originating in tropical Africa and South America, which is transported around the tropics and mixed into the extratropics. This plume, sometimes punctuated by biomass burning emissions from Australia and Southeast Asia, is thought to generally determine the variability of CO in remote parts of New Zealand and in Antarctica [*Zeng et al.*, 2012]. The important role played by biomass burning and large-scale meteorological features, combined with low emission totals for anthropogenic CO compared to the Northern Hemisphere, means that CO in the Southern Hemisphere is characterized by long-range transport and large-scale variations [*Edwards et al.*, 2006a, 2006b].

[4] Here we assess the large-scale variability of Southern Hemisphere CO. One could conceivably address this issue using the global CCGG network of in situ flask sampling measurements (http://www.esrl.noaa.gov/gmd/flask.html). For the study of long-range correlation, however, this measurement type is not ideal because of often substantial local and boundary-layer influences on these measurements and because of the relatively low frequency of measurements (typically once a week to once a month). Hence here we focus on FTIR, satellite, and model data and address the question of how representative the Lauder and Arrival Heights FTIR measurements of CO are for the southern extratropics. Arrival Heights and Lauder are the southernmost

[1]National Institute of Water and Atmospheric Research, Lauder, New Zealand.
[2]Formerly at National Institute of Water and Atmospheric Research, Lauder, New Zealand.
[3]Center for Atmospheric Chemistry, School of Chemistry, University of Wollongong, Wollongong, New South Wales, Australia.

Corresponding author: O. Morgenstern, National Institute of Water and Atmospheric Research, Private Bag 50061, Omakau 9352, New Zealand. (olaf.morgenstern@niwa.co.nz)

0148-0227/12/2012JD017639

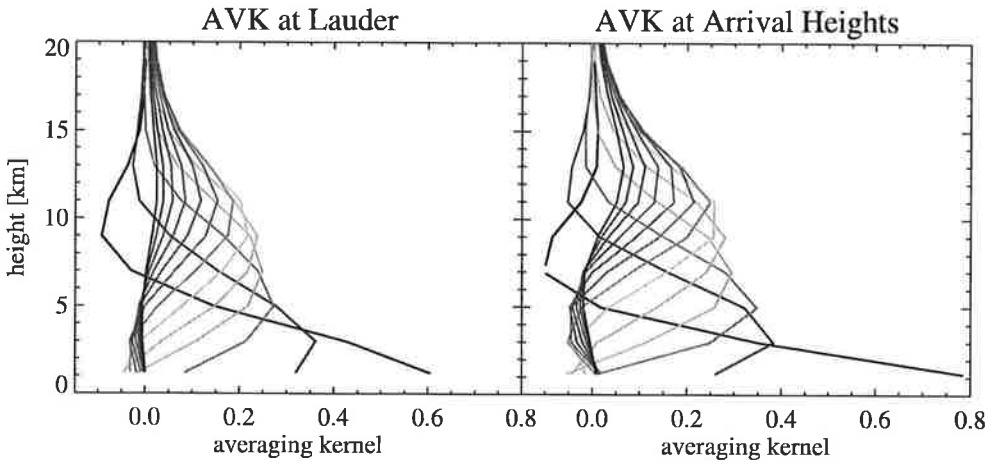

Figure 1. Averaging kernels for the (black) 1.2 km, (dark blue) 3 km, (light blue) 5 km, (dark green) 7 km, (light green) 9 km, (yellow) 11 km, and higher nominal levels for the Fourier transform infrared (FTIR) instruments, at Lauder and Arrival Heights. The averaging kernels have been averaged in time over 1997–2010. The averaging kernels extend to 90 km.

FTIR instruments of the network, surrounded mostly by ocean and ice. They are considered clean-air sites where variability is governed by intercontinental transport [*Edwards et al.*, 2006a] with little or no in situ production. This makes them ideal reference stations for satellite validation studies [e.g., *de Laat et al.*, 2010]. We compare the FTIR data to the Measurements of Pollution in the Troposphere (MOPITT) satellite CO column data [*Drummond and Mand*, 1996; *Bowman*, 2006; *Edwards et al.*, 2006a, 2006b] and a chemistry-climate model (CCM) simulation [*Zeng et al.*, 2008]. Using these data, we investigate similarities and differences between the data sets and their respective limitations. We use a correlation analysis to assess spatial coherence in the data. In a generalization of the analysis, we assess how representative areas of the globe are regarding column CO and where, from a pure science perspective, a new FTIR instrument might be advantageously sited. We assess potential causes of differences between the measurement platforms and between the measurements and the model.

[5] For comparison and completeness, we also show measurements of CO total columns made at Wollongong.

2. Data

2.1. Ground-Based FTIR Measurements of CO Column

[6] CO column measurements using a ground-based FTIR instrument are possible only during the day and under clear conditions, as the FTIR measures absorption lines in the infrared part of the solar spectrum. Hence, at Arrival Heights, there is a data gap of 4–5 months during each polar night. The measurements at Arrival Heights were made using a Bruker 120M FTIR spectrometer [*Wood et al.*, 2002]. The measurements at Lauder [*Griffith et al.*, 1998] were initially made with a similar 120M but were changed to a 120HR Bruker model in September 2001. Both instruments have the same maximum optical path difference of 257 cm, resulting in a spectral resolution of 0.0035 cm^{-1}. Mirror tracking systems were used to record direct sun spectra in the midinfrared (2–14 μm), using liquid nitrogen–cooled detectors. The retrieval of trace gas information from these recorded spectra was performed using version 3.93 of the profile retrieval algorithm SFIT2 and is similar to that described by *Rinsland et al.* [1998, 2002]. CO is retrieved from a spectral window centered around 5 μm. Only during spring is there a noticeable contribution from middle and upper atmosphere CO to the total column at Arrival Heights [*Velazco et al.*, 2007]. Figure 1 shows the FTIR averaging kernels at the Lauder and Arrival Heights sites. Despite the large separation in latitude, and some minor differences between the two instruments, the averaging kernels (and hence the measurement characteristics) of the two sites are remarkably similar.

[7] *Griffith et al.* [1998] and *Paton-Walsh et al.* [2004, 2005] give details on the Wollongong FTIR instrument and processing method.

2.2. MOPITT Measurements of CO Column

[8] We use near-global measurements of total CO columns made by the Measurements Of Pollution in the Troposphere (MOPITT) satellite-based instrument (ftp://l4fl01.larc.nasa.gov/MOPITT/MP03.004). The original resolution of the level 2 data is 22 km [*Drummond and Mand*, 1996] (the version 4, level 3, data used here are gridded to a 1° × 1° resolution). The data span 3 March 2000 to 4 August 2011 and comprise separate daytime and nighttime measurements. Broadly, the measurements cover the region equatorward of ±85°. At every grid cell and time covered by measurements, a single-measurement precision σ and number of measurements ("pixels") n of the data are given, reflecting the reproducibility of the data. Assuming that the "noise" is Gaussian, from this we infer a data precision $\epsilon = \sigma/\sqrt{n}$. Figure 2 shows the mean relative precision (i. e., ϵ divided by the grid point mean CO column) as well as a density plot of the spread of errors. The figure suggests that nighttime data are of slightly inferior quality (except for the northern midlatitudes, which are more precisely sampled during the day than at night), and the data quality deteriorates significantly poleward of ±60°. At middle and low latitudes, the precision is typically of the

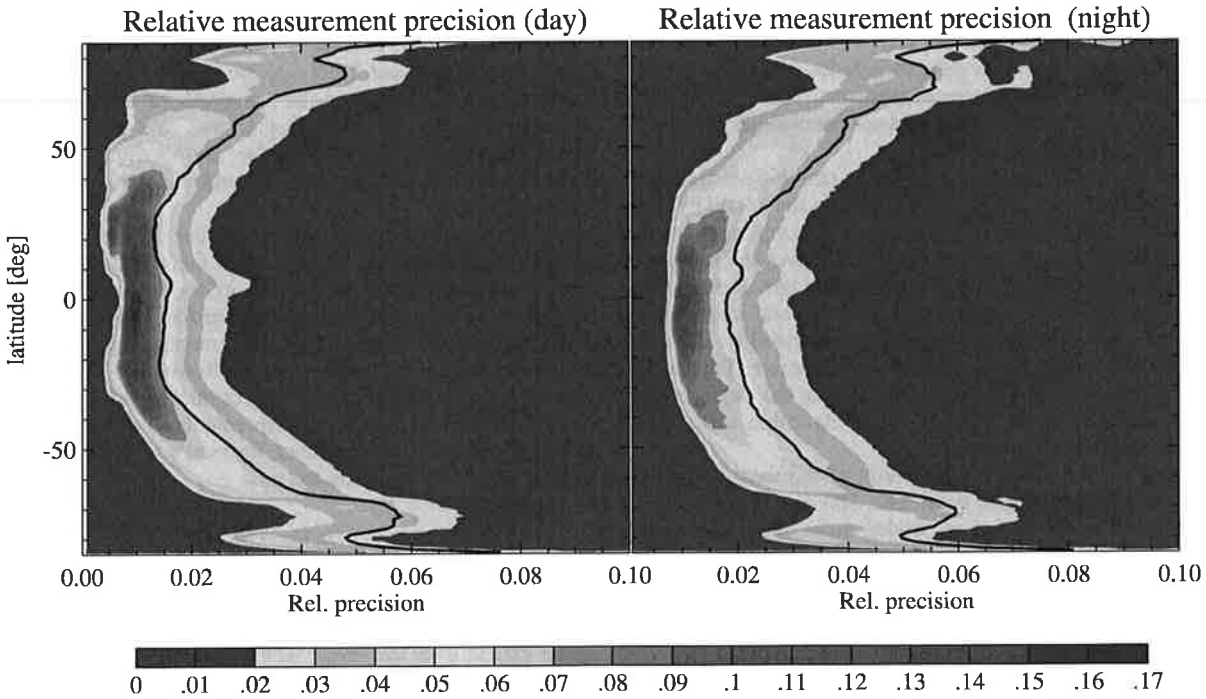

Figure 2. Solid line indicates mean relative precision $\epsilon = \sigma/\sqrt{n}$ for (left) daytime and (right) nighttime Measurements of Pollution in the Troposphere (MOPITT) measurements. Colors indicate density plot of probability density function (arbitrary units) of the precision.

order of a few percent but increases substantially toward high latitudes. The filling ratio (i.e., the fraction of grid points covered by MOPITT data) is about 12% with daytime and 16% with nighttime data. For 3% of grid points both daytime and nighttime data are available. There are also some periods without measurements in the version 4 MOPITT data.

[9] An inspection of the averaging kernels of the daytime and nighttime MOPITT measurements (Figure 3) suggests

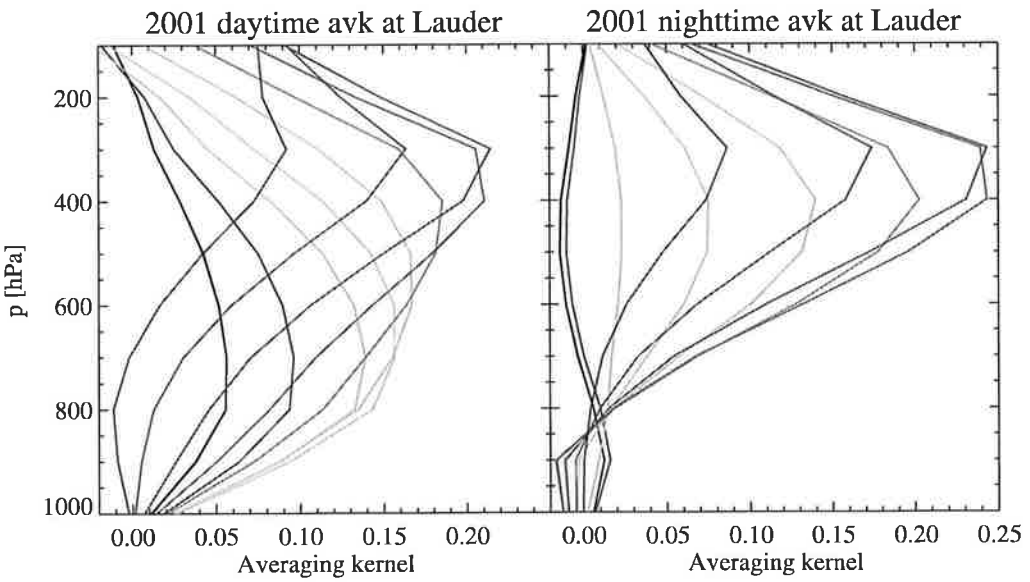

Figure 3. Averaging kernels for the MOPITT data at the grid point closest to Lauder (169.5°E, 45.5°S), averaged over the year 2001, for the (left) daytime and (right) nighttime measurements. Colors indicate the averaging functions for the 10 nominal pressure levels (surface, 900 to 100 hPa with a spacing of 100 hPa) representing the MOPITT profiles.

that measurement characteristics, at least at the Lauder grid point, differ appreciably between the two data sets, with nighttime measurements substantially less sensitive to near-surface CO than daytime measurements [*Deeter et al.*, 2003, 2007]. For this reason, in the analysis detailed below we only use daytime measurements.

[10] For an analysis of long-range correlations it is necessary to use interpolation to fill gaps in the MOPITT data, so that two time series with nonmatching sampling times can be paired up for the analysis. Figure 4 shows an example of the original MOPITT data (Figure 4a) and two domain-filled versions. The version based on spatiotemporal interpolation (Figure 4b) exhibits less grid-scale variability than the equivalent using only temporal interpolation (Figure 4c). For this reason, in the following we use the daytime only data, subjected to the domain-filling algorithm using linear spatiotemporal interpolation.

[11] Figure 5 illustrates the result of the data filling process for the Lauder grid point for a 100 day period in 2009. The figure suggests that at Lauder, quite often the interpolated CO column lies outside the range of uncertainty of the nighttime CO measurements. This is not a surprise, considering the aforementioned differences in the averaging kernels (Figure 3) and the reduction in variability associated with interpolation. For comparison to the CCM (see below) we also generate a reduced-resolution version of the data set at 3.75° × 2.5°, by taking the average of the high-resolution data at every low-resolution grid cell.

2.3. The CCM Simulation

[12] The model simulation used here is performed using the UMCAM global tropospheric CCM which has been extensively used and validated [e.g., *Zeng et al.*, 2008, 2010]. *Zeng et al.* [2012] use the same simulation. The model covers the atmosphere below 4.6 hPa with 19 levels at a horizontal resolution of 3.75° × 2.5°. In this study, we use a transient simulation of tropospheric chemistry driven with observed Atmospheric Model Intercomparison Project Phase 2 (AMIP2) sea surface temperature and sea ice conditions (http://www-pcmdi.llnl.gov). Thirteen years of daily-mean column CO fields are used in this study, covering 1997 to 2009. Emissions of ozone precursors represent present-day conditions with no year-to-year variations as used by *Zeng et al.* [2008], with the exception of biomass burning emissions, which follow the GFED v3.0 data set [*van der Werf et al.*, 2010].

[13] In comparison with the approach used by *Zeng et al.* [2008], we reduce the total amount of isoprene emissions from 560 Tg/yr [*Guenther et al.*, 1995] to 390 Tg/yr. This emission total is within the range of emission totals assumed in the recent literature [*Arneth et al.*, 2011] and produces a better match of modeled and observed CO columns. A separate paper on this aspect is in preparation.

3. Method

[14] Similar to the method used by *Rinsland et al.* [2002], we fit, using least squares regression, a trigonometric polynomial and trend term of the form

$$y(t) = y_0 + mt + \sum_{n=1}^{3} y_n \sin(2\pi nt + \varphi_n) + \mu(t) \qquad (1)$$

to the CO column data, where y_0 is a constant offset, m is the linear trend, t is time in units of years, with $t = 0$ denoting the beginning of the year 1997, φ_n are the phases of the CO column signal, and $\mu(t)$ is the remainder of the signal not captured by the previous five terms. We perform this regression separately for Lauder and Arrival Heights, defining the Lauder residual $\mu_L(t)$ and the Arrival Heights residual $\mu_{AH}(t)$.

[15] Next we focus on the remainder terms $\mu_L(t)$ and $\mu_{AH}(t)$ in equation (1), which reflect the remaining inadequacies in the expansion, as well as the interannual variability of the CO signal. Noting that the Arrival Heights time series is more sparsely sampled and contains gaps for every austral winter, for lag times τ ranging from 0 to 100 days, we linearly interpolate the Lauder CO residual μ_L onto the times for which Arrival Heights measurements of CO are available, shifted by τ, and calculate Pearson's correlation coefficient as a function of the lag time τ:

$$C(\tau) = \frac{\langle \mu_L(t-\tau) | \mu_{AH}(t) \rangle}{\| \mu_L \| \cdot \| \mu_{AH} \|} \qquad (2)$$

In the above, $\langle x|y\rangle = \sum_i x_i y_i$ and $\| x \| = \sqrt{\langle x|x\rangle}$, and both sums extend over the range where the shifted Lauder time series lies within the range of times spanned by the Arrival Heights data.

[16] Similar analyses are also applied to the UMCAM simulation results and the domain-filled MOPITT satellite data. In both cases, the instantaneous observations are replaced with daily-mean data. Furthermore, for the satellite and model data, because these data are regularly gridded in time, we replace the parametric regression form of equation (1) with a nonparametric mean annual cycle and linear trend term. For the MOPITT data, we assume a year length of 365 days and omit 29 February of 2004 and of 2008 from the time series. The UMCAM simulation has been performed assuming a 360 day calendar without leap years. For both data sets, the lagged correlation analysis is extended globally, i.e., we calculate the lag and the correlation of the Lauder and Arrival Heights CO residuals with all other grid points.

4. Results

4.1. Comparison of FTIR, MOPITT, and Model Results

[17] Figure 6 shows the time series of CO total columns for Lauder, Arrival Heights, and Wollongong from the FTIR instruments, MOPITT, and the UMCAM CCM. For Arrival Heights, the FTIR data exhibit a significant downward trend [*Zeng et al.*, 2012], which does not occur in the MOPITT data. Also, here the satellite tends to overestimate the FTIR measurements during the spring season. The model captures aspects of the interannual variability, particularly the anomalous summer of 1998 caused by wildfires in Indonesia [*Rinsland et al.*, 1999], but underestimates the size of the annual cycle.

[18] At Lauder, both the satellite and the model well match the FTIR measurements. The model again captures aspects of the annual cycle and some of the variability, particularly in 1998. However, the model does not represent the extreme events seen in the FTIR data. The model has too weak a

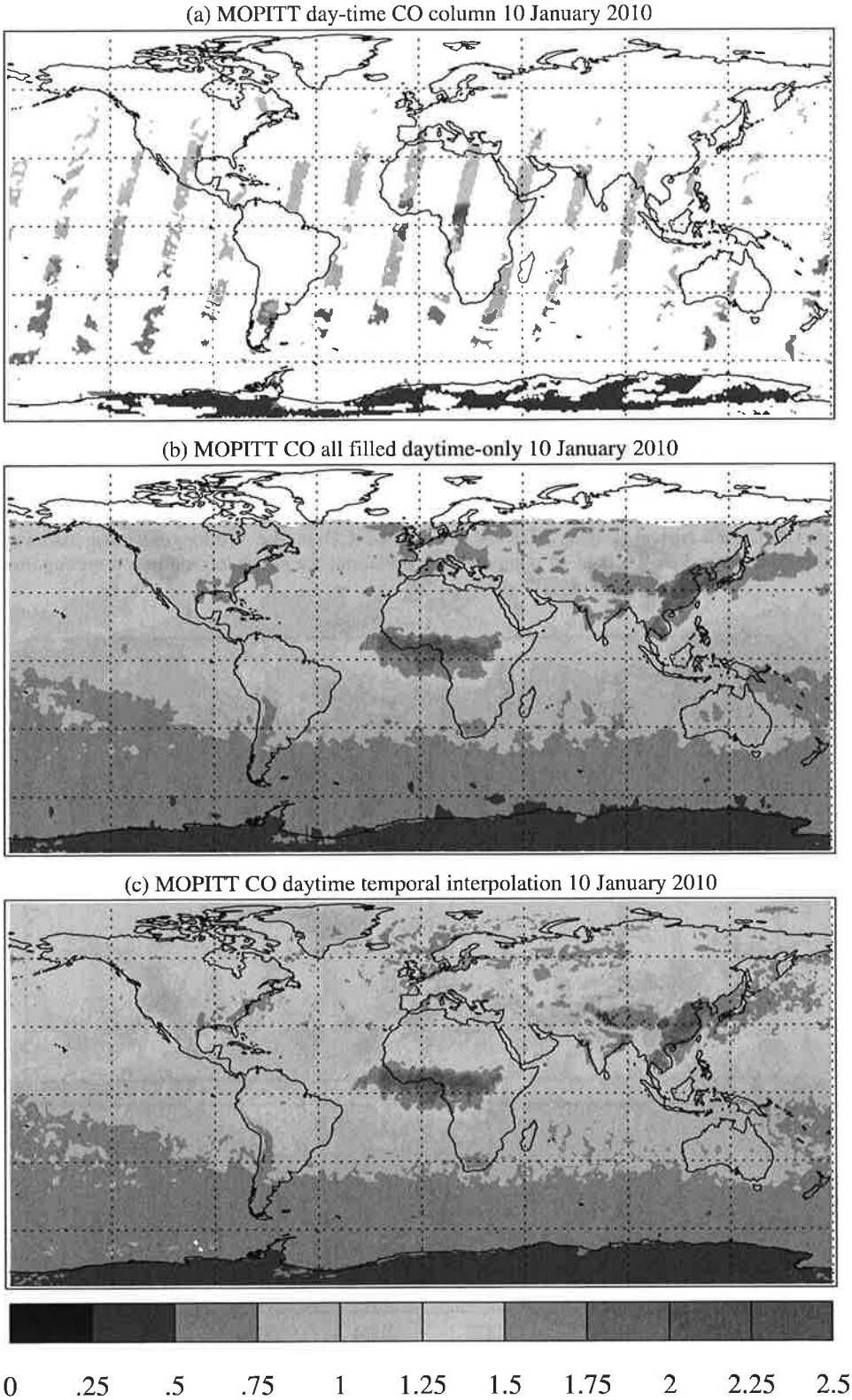

Figure 4. Daytime MOPITT CO column (10^{18} molecules/cm^2) for 10 January 2011. (a) Version 4, level 3, daytime measurements at 1° × 1° resolution. (b) Filled data set at 1° × 1° using spatiotemporal interpolation. (c) Filled data set, using only temporal interpolation.

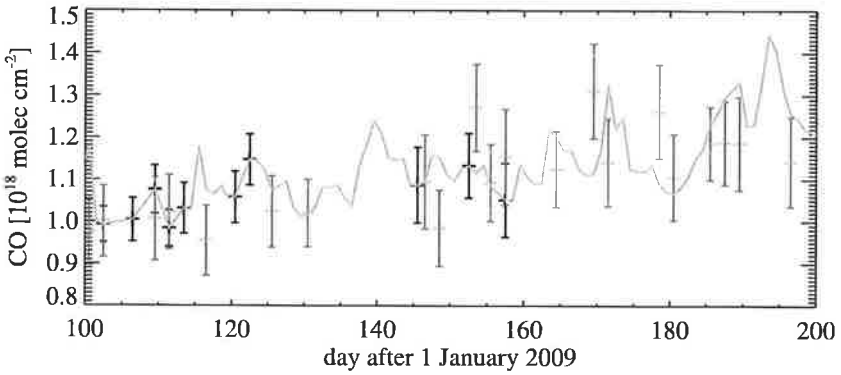

Figure 5. MOPITT CO column data for the grid point closest to Lauder, for 100 days of the year 2009. Black, daytime CO measurements with associated error bars; yellow, nighttime CO measurements; and green, domain-filled CO based on daytime data.

latitudinal gradient of CO between Lauder and Arrival Heights in summer.

[19] The Wollongong FTIR data broadly corroborate the findings based on Lauder and Arrival Heights FTIR data in that there is a downward trend in the data of comparable magnitude to Lauder, and the seasonal cycle is nearly in phase with Lauder. However, in contrast to the Lauder and Arrival Heights data, there are spikes of substantially elevated CO in the Wollongong data associated with local pollution; the site is located near a metropolis (Sydney) and

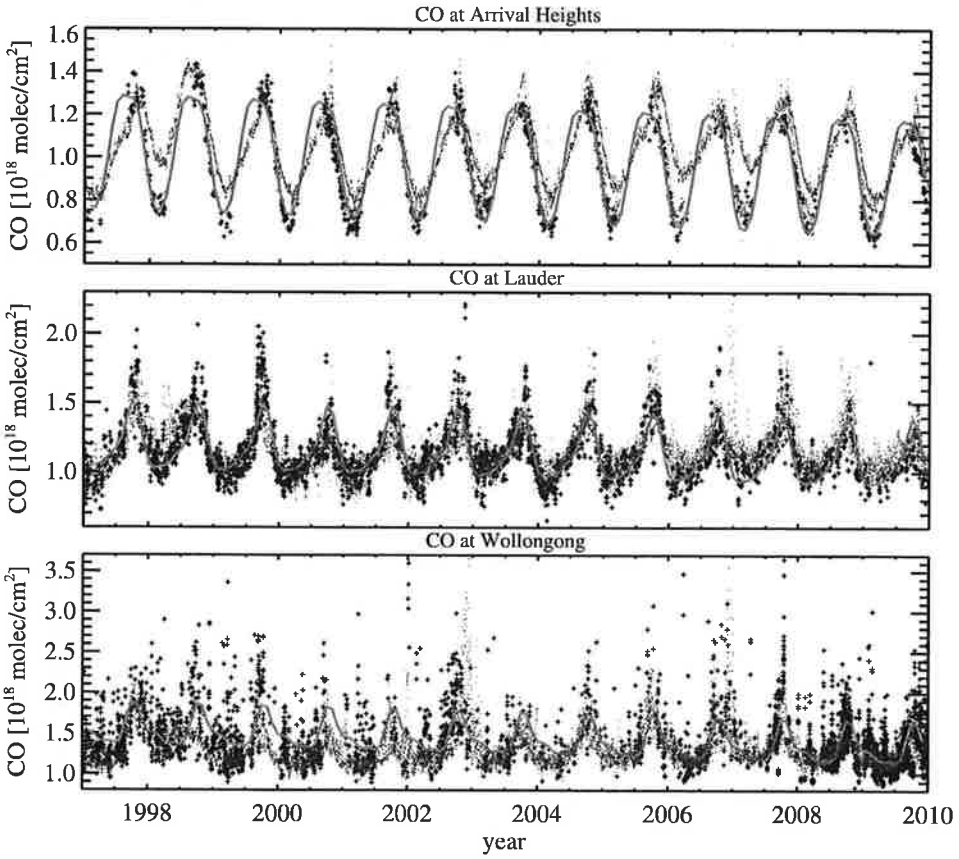

Figure 6. CO column data at (top) Arrival Heights (middle) Lauder, and (bottom) Wollongong. Black symbols: FTIR total column CO measurements. Green dots: MOPITT daytime total column data, evaluated at the grid points closest to the stations. Blue: UMCAM. Orange solid line: Linear trigonometric regression to the FTIR data following equation (1).

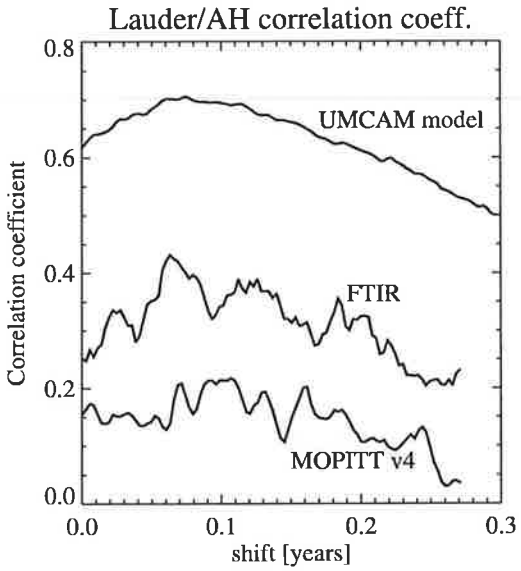

Figure 7. Pearson's correlation coefficient of Arrival Heights and Lauder CO column data, as a function of lag time between the Lauder and Arrival Heights data, for the UMCAM model, FTIR, and MOPITT. The Lauder data have been shifted by the lag time time and interpolated onto the times of the Arrival Heights data.

also near heavy steel industry. Because of these local effects we do not use the Wollongong data in the following long-range correlation analysis.

4.2. Transport Time Scales and Lagged Correlation Analysis

[20] Next we focus on the lagged-correlation analysis described in section 3. Figure 7 shows the correlation coefficient $C(\tau)$ defined in equation (2) between Lauder and Arrival Heights, for the UMCAM, FTIR, and MOPITT data. For no lag, the FTIR data indicate that the correlation coefficient is about 0.25. The correlation maximizes at a lag of 0.06 years or 22 days; the maximum correlation coefficient is about 0.44.

4.2.1. Model Results: Lagged Correlations in CCM Data

[21] The lagged correlation between Lauder and Arrival Heights CO columns, as modeled by UMCAM, suggests a systematically larger correlation than that obtained from FTIR for the range of lags investigated here, and much reduced variability (Figure 7). We extend the analysis to pairs of model grid points not generally covered by FTIR data. Figure 8 shows maps of lagged correlation (maximized with respect to the lag time τ), derived from the UMCAM model results, at Lauder, Arrival Heights, Bremen (Germany) and Eureka (Canada), with all other grid points elsewhere on their respective hemispheres. The maps show that Lauder correlates at 0.6 or more with much of the Southern Ocean and all of Antarctica. Arrival Heights correlates at 0.8 or more with almost the whole region south of 60°S and at 0.6 or more with almost the whole Southern Hemisphere except for the continents of Africa and South America and neighboring seas. By contrast, the station of Bremen is representative, at a correlation coefficient 0.6 or better, only for a relatively small region comprising western central Europe, the British Isles, and a portion of the eastern North Atlantic. Eureka, located in remote Arctic Canada, is representative mostly of the Arctic Ocean and portions of the northern continents.

[22] Corresponding lag times are displayed in Figure 9. For the midlatitude stations Lauder and Bremen, which are located in generally westerly wind regimes, lag times are consistently increasing from west to east, indicating that the CO signal is composed of anomalies passing over these stations with the westerly flow. For Lauder, this region of coherent eastward transport covers a substantial portion of the southwestern Pacific. It is bounded to the north and south by regions outside the storm track, where the lag times change discontinuously, but still these regions (north of ~30°S and south of ~60°S) correlate at over 0.6 with the Lauder signal. For Arrival Heights, the model also suggests the existence of a westerly flow zone which comprises much of the Pacific sector of Antarctica; this region is again bounded by about ~60°S. To the north of this, lag times exceeding 10 days ensue. The modeled Eureka time series correlates at 0.6 or more with much of the Arctic but the lag times appear somewhat incoherent, possibly because Eureka is not located in a predominantly westerly flow regime.

4.2.2. Analysis of Areas of Increased Correlation

[23] In the above analysis, we have calculated, using the UMCAM model data, that the CO columns modeled for the Lauder and Arrival Heights locations correlate highly with substantial portions of the Southern Hemisphere. These two locations were picked because there are FTIR instruments located there. The analysis results corroborate earlier findings; e.g., *Duncan and Logan* [2008] show that CO columns at high southern latitudes are to a large extent governed by transport from the tropics.

[24] We extend the analysis to every grid point and calculate a correlation length, which is defined as the square root of the surface area of the portion of the globe where CO columns correlate at 0.6 or more with those at any chosen grid point. The result is shown in Figure 10. Lauder and Arrival Heights, the two southernmost stations in the FTIR network, are characterized by larger correlation lengths than any other FTIR station. However, the regions of greatest interest, globally, are not covered by the network. These are the southern subtropical Pacific, where the correlation length maximizes, and parts of South and East Asia, southern subtropical Africa, and the eastern United States, where the correlation length minimizes. Due to its remoteness and long transport times from major emission areas, the southern subtropical Pacific region would be particularly suitable for a hypothetical additional FTIR station aiming to capture large-scale features in CO affecting the Southern Hemisphere.

4.2.3. Long-Range Correlation Analysis on MOPITT Data

[25] We compare these results with the corresponding calculations using the MOPITT data. The results are shown in Figure 11. For Bremen, the shape and size of the high-correlation anomaly surrounding the site agrees reasonably well with the one found in the model data. The area with correlations exceeding 0.4 in the MOPITT data is similar to the area with correlations exceeding 0.6 in the model. Also, the very low correlation with southern and eastern Asia is

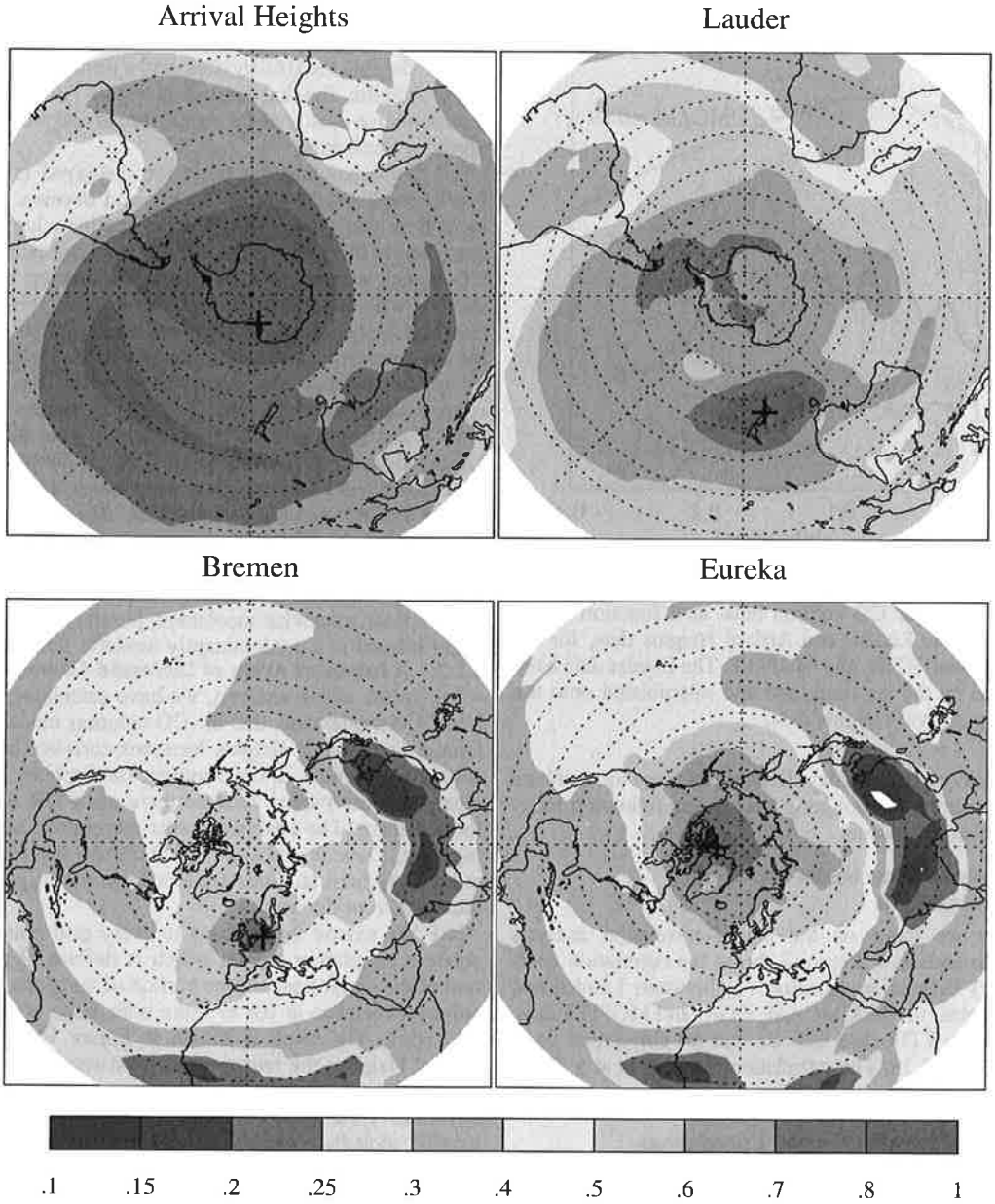

Figure 8. Correlation coefficient of the modeled CO column, taken at the Lauder, Arrival Heights, Bremen (Germany), and Eureka (Canada) grid points, with the CO columns elsewhere on their hemispheres. The correlation has been optimized with respect to the lag time τ.

captured. The correlation is generally larger in the model than in the MOPITT data. In particular, the large correlation in the model of Bremen CO with CO in the Arctic region is not found in the MOPITT data. For Lauder, like in the model, we find an increased correlation with much of the Southern Ocean, also extending into the South Atlantic, but again the correlation coefficients are smaller than in the model. The high correlation with southern high latitudes apparent in the simulation does not occur in the MOPITT data. For the high-latitude stations Eureka and Arrival Heights, in both cases the large correlations with their respective polar caps is not reflected in the MOPITT data, and the shapes of the high-correlation areas look substantially different (not shown). The anomalously low correlations of the Lauder grid point with parts of Amazonia are likely the consequence of poor sensitivity of the MOPITT instrument over tropical rain forest [*Deeter et al.*, 2007].

4.3. Analysis of Model-Measurement Differences

[26] The results suggest that long-range correlations are systematically smaller for both the MOPITT and FTIR data than in the UMCAM model results, particularly in the case

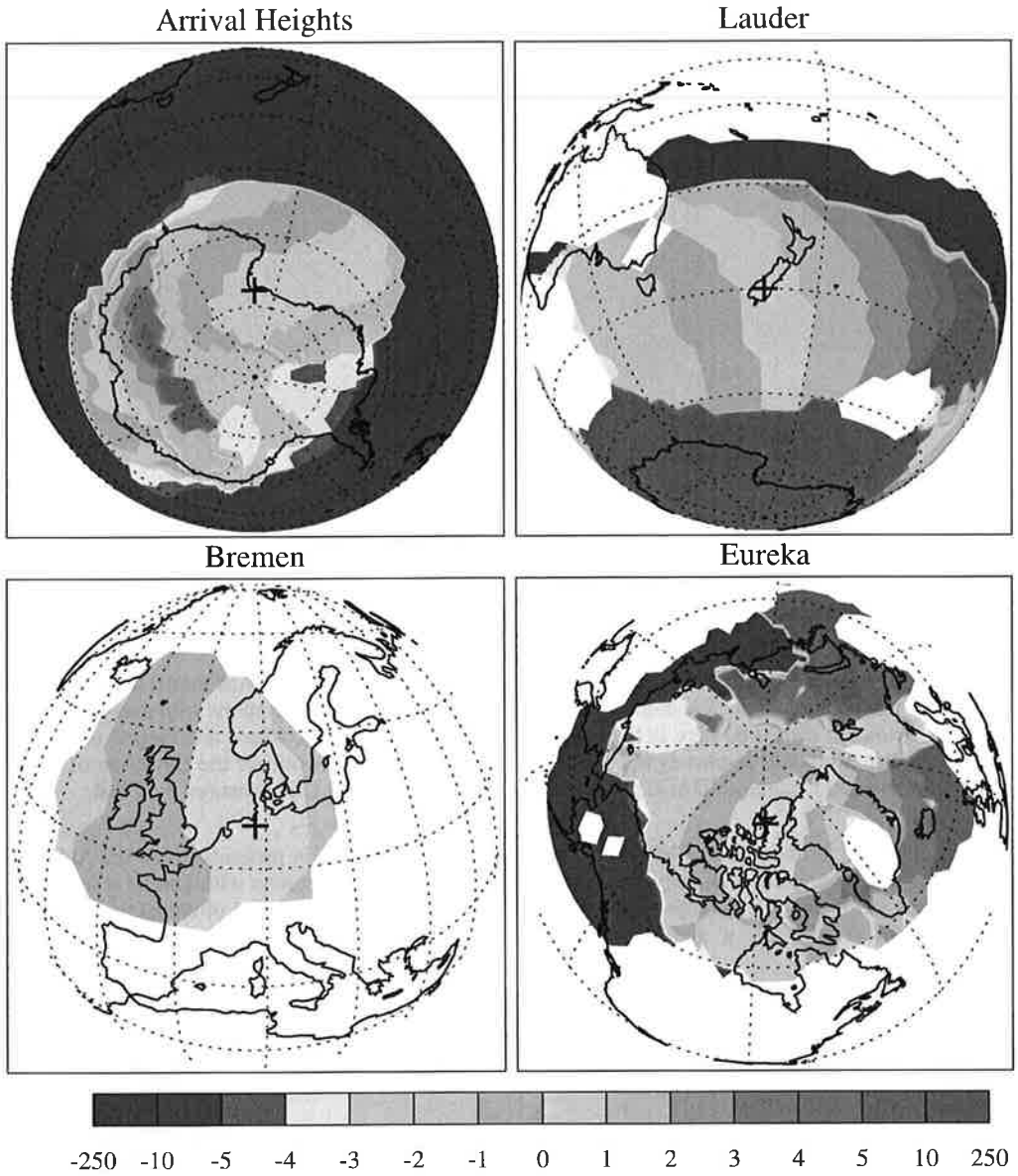

Figure 9. Lag time τ (days) associated with the optimized correlation displayed in Figure 8, for Lauder, Arrival Heights, Bremen, and Eureka, from the UMCAM model results. Regions not covered in color correspond to correlation coefficients with the corresponding station grid point of less than 0.6.

of MOPITT, in polar areas. For a comparison of remote sensing (such as MOPITT and FTIR) and model data, it is generally recommended that the model data are folded with corresponding averaging kernels and a priori data (as in equation (3)) to mimick what the remote sensing instrument would see if the model data represented the real atmosphere [e.g., *Rodgers and Connor* 2003]:

$$x' = x_{ap} + \mathbf{A}(x - x_{ap}) \tag{3}$$

Here x is a modeled profile of CO, x_{ap} is some corresponding a priori data (produced by an independent model and annually repeating), $\mathbf{A}$ is the averaging kernel matrix, and x' is the profile that would have been measured by the instrument if x were the real profile of CO. As shown in Figure 3, the near-surface sensitivity to variations in CO of the MOPITT instrument is small.

[27] We apply equation (3) to the UMCAM model data, using MOPITT daytime averaging kernels and a priori data. For this, we follow the procedure laid out in the MOPITT user guide (http://www.acd.ucar.edu/mopitt/v4_users_guide_val.pdf). The thus produced profiles x' have the same coverage in space and time as the MOPITT level 3 daytime data. We then subject the resulting modified profiles x' to

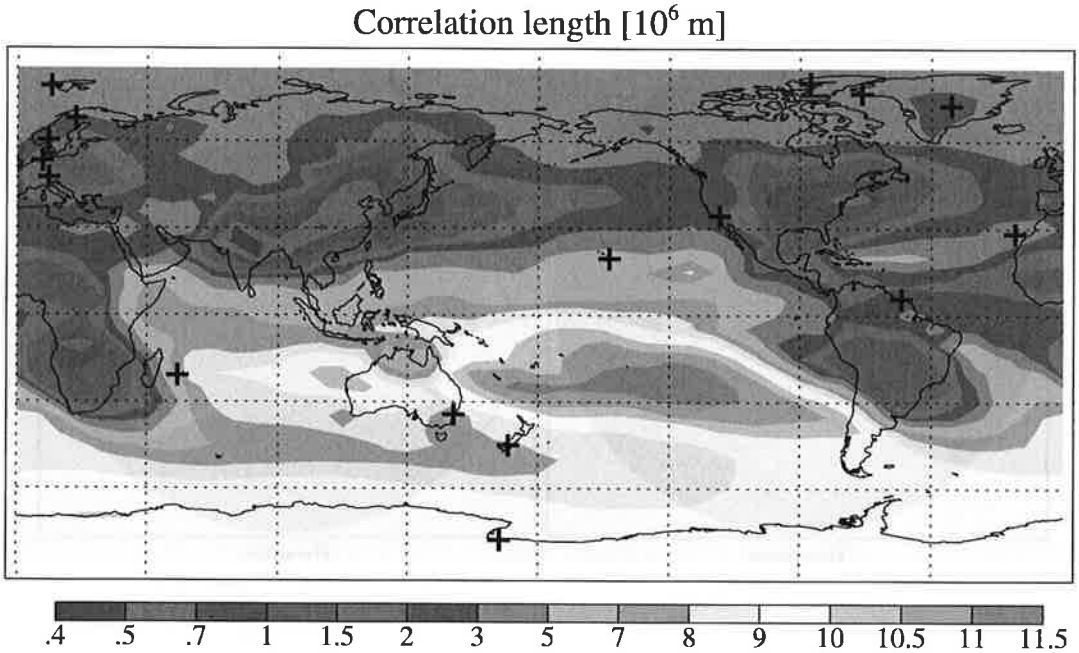

Figure 10. Correlation length (in 10^6 m) in the UMCAM CO field. The UMCAM model data have been subsampled to a 7.5° × 5° grid. For every grid point, maximized lagged correlations with every other grid point are calculated; displayed here is the square root of the surface area where this lagged correlation exceeds 0.6. Superimposed in plus symbols are the locations of the Network for the Detection of Atmospheric Composition Change (NDACC) stations reporting total column CO measured by FTIR.

the same domain filling algorithm as the MOPITT data, and evaluate the long-range correlations as explained above. The result is displayed in Figure 12. In comparison with the unmodified model data (Figure 8), a generally reduced correlation ensues. In particular, over the Antarctic continent the long-range correlation with Lauder is lost. As this feature is bounded by the coastline of Antarctica, it is an expression of a general lack of sensitivity of the MOPITT instrument

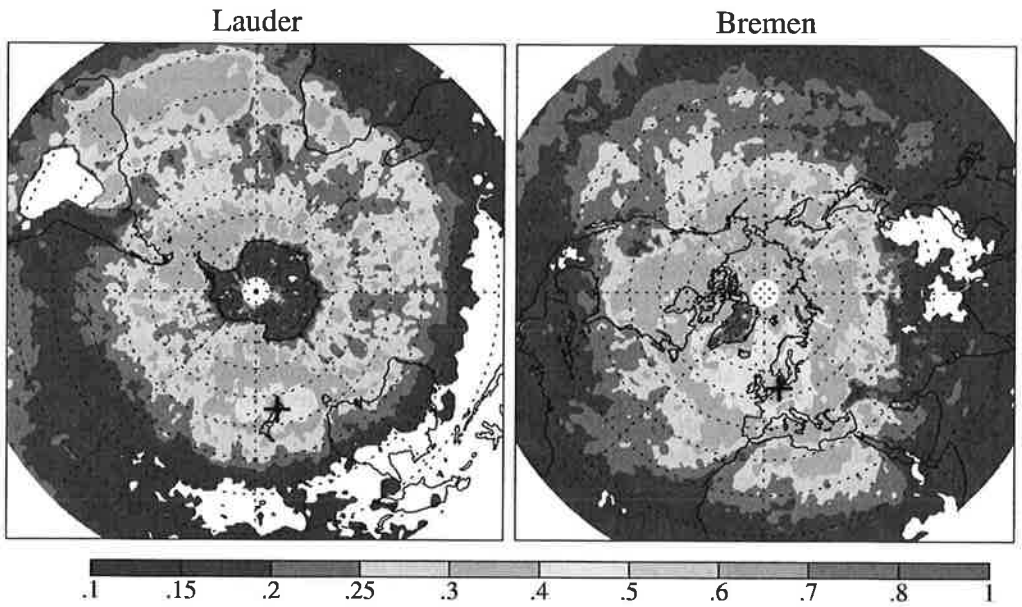

Figure 11. Same as Figure 8 but using the domain-filled MOPITT data at a 1° × 1° resolution, for Lauder and Bremen.

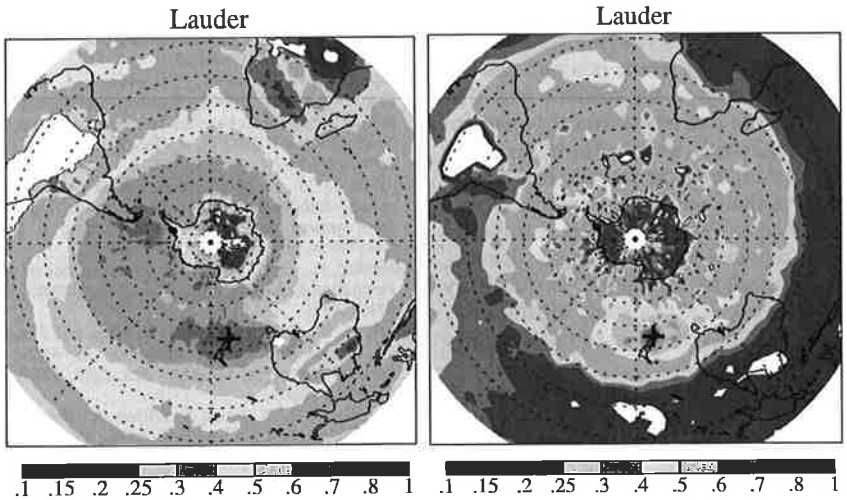

Figure 12. Lagged correlation maps with the Lauder grid point, for (left) UMCAM data, regridded to the MOPITT grid and folded with the averaging kernel and a priori data of the MOPITT data (see text for details), and (right) domain-filled MOPITT data, regridded to 3.75° × 2.5°.

over cold surfaces (http://eosweb.larc.nasa.gov/PRODOCS/mopitt/Quality_Summaries/mopitt_level2_ver4.html). *Warner et al.* [2010] report a general reduction in the degrees of freedom with increasing absolute latitude in the MOPITT data; this is not obviously reflected in the long-range correlations. For example, there is a considerable reduction of the correlation of Lauder column CO with that over the southern subtropical oceans, whereas there is only a small reduction in the correlation with CO over the Southern Ocean (cf. Figures 11 and 12).

[28] We perform the above manipulation (equation (3)) for the FTIR data, using the FTIR averaging kernels (Figure 1). The result is that the original model column amounts derived from x correlate very highly with the modified column data derived from x' (not shown). This suggests that the long-range correlations in total column CO are generally unaffected by the application of FTIR averaging kernels. For the FTIR instruments, this measurement limitation therefore does not explain the somewhat lower long-range correlation between Lauder and Arrival Heights in the measurements, compared to the model.

[29] A further obvious difference between the model and the MOPITT measurements is that the MOPITT data come at a higher spatial resolution, suggesting larger random noise in the MOPITT than the model data. To assess the significance of this factor, we have regridded the domain-filled MOPITT data to the model grid and repeated the lagged-correlation calculation at the lower resolution. The result is displayed in Figure 12. For the spatially degraded MOPITT data, lagged correlations are very similar to those at the original resolution but with generally increased correlation coefficients around the Southern Ocean. Regions that at the original high resolution do not correlate with the Lauder data, i.e., much of the tropics and Antarctica, remain largely unaffected by the change in resolution. Around the Southern Ocean, the correlation with the Lauder data increases from typically 0.2–0.3 to around 0.3–0.4. Both measures combined explain some of the difference in long-range correlations in the model versus MOPITT data.

5. Discussion and Conclusions

[30] The Arrival Heights time series is sparsely sampled (there are around 800 measurements in the series), and there are data gaps during the polar nights. Furthermore, in calculating the lagged correlation, the Lauder data, shifted by the lag, are interpolated onto the Arrival Heights sampling times. We assess whether these properties affect the correlation of the two sites, by subsampling the UMCAM model data at the measurement times and the locations of the two stations, then repeat the same analysis as shown above on the measured data. The result is a largely unchanged, substantial correlation between the two sites. Likewise, we have established that perturbing the model data at the two sites with a normally distributed random error of a 1% standard deviation (a conservative estimate of the mean error in the FTIR data) does not appreciably affect the correlation between them. We thus conclude from these experiments that the overestimation of the modeled lagged correlation between the two sites likely reflects the model's numerical diffusivity, its inability to represent small scales, erroneous transport, or deficiencies in the imposed emissions. This might also explain the seasonally weak latitudinal gradient in CO between Lauder and Arrival Heights noted before. Nonetheless, the lagged correlation between the two sites found in the FTIR data is substantial. Both model and FTIR data (Figure 7) suggest that this lagged correlation generally undergoes a very broad maximum, with essentially unchanged correlations for lag times between 15 and 40 days. This range of lag times presumably reflects variability in transport as well as mixing effects.

[31] The substantial lagged correlation of the CO column time series at Lauder and Arrival Heights is found in the FTIR data and in the model, but less so in the satellite MOPITT CO observations. We have designed two sensitivity

experiments to address the causes of this discrepancy: We have assessed the effect of applying averaging kernel to the model data, mimicking the measurement process, and we have regridded the MOPITT data to the model's grid. The sensitivity experiments indicate that measurement limitations expressed by the averaging kernels, and the lower resolution of the model, partially explain why the satellite data do not show this long-range correlation across the Southern Ocean. The remainder is likely due to instrument noise and meteorological variability not captured by the averaging kernels, and to model imperfections such as its diffusivity and inability to represent small scales. Also, inaccurate and insufficiently variable emissions and issues with transport of CO are likely to contribute to this problem.

[32] The weaknesses in satellite observations and in chemistry-climate modeling found above point at the crucial role that FTIR measurements can play in tracking transport and dispersion of tropospheric pollution. They are important for validating model results, and also for benchmarking satellite data [*de Laat et al.*, 2010]. Usage of satellite data can be complicated by insufficient sensitivity, particularly at high latitudes and in relatively clean Southern Hemisphere air.

[33] **Acknowledgments.** We thank the New Zealand Ministry of Science and Innovation for funding this research under the DMGC program. We also thank the Australian Research Council for funding the Wollongong measurements as part of the project DP110101948. We acknowledge the UK Met Office for use of the Unified Model. Furthermore, we acknowledge usage of MOPITT version 4 data which were obtained from the NASA Langley Research Center Atmospheric Science Data Center.

References

Arneth, A., G. Schurgers, G. J. Lathière, T. Duhl, D. J. Beerling, C. N. Hewitt, M. Martin, and A. Guenther (2011), Global terrestrial isoprene emission models: Sensitivity to variability in climate and vegetation, *Atmos. Chem. Phys.*, *11*, 8037–8052, doi:10.5194/acp-11-8037-2011.

Bowman, K. P. (2006), Transport of carbon monoxide from the tropics to the extratropics, *J. Geophys. Res.*, *111*, D02107, doi:10.1029/2005JD006137.

Chatfield, R. B., Z. Guo, G. W. Sachse, D. R. Blake, and N. J. Blake (2002), The subtropical global plume in the Pacific Exploratory Mission-Tropics A (PEM-Tropics A), PEM-Tropics B, and the Global Atmospheric Sampling Program (GASP): How tropical emissions affect the remote Pacific, *J. Geophys. Res.*, *107*(D16), 4278, doi:10.1029/2001JD000497.

Crutzen, P. J., and G. R. Carmichael (1993), Modeling the influence of fires on atmospheric chemistry, in *The Environment: The Ecological, Atmospheric, and Climate Importance of Vegetation Fires*, edited by P. J. Crutzen and J. G. Goldammer, pp. 90–105, John Wiley, Hoboken, N. J.

Crutzen, P. J., L. E. Heidt, J. P. Krasnec, W. H. Pollock, and W. Seiler (1979), Biomass burning as a source of atmospheric gases CO, H_2, N_2O, NO, CH_3Cl and COS, *Nature*, *282*, 253–256, doi:10.1038/282253a0.

Deeter, M. N., et al. (2003), Operational carbon monoxide retrieval algorithm and selected results for the MOPITT instrument, *J. Geophys. Res.*, *108*(D14), 4399, doi:10.1029/2002JD003186.

Deeter, M. N., D. P. Edwards, J. C. Gille, and J. R. Drummond (2007), Sensitivity of MOPITT observations to carbon monoxide in the lower troposphere, *J. Geophys. Res.*, *112*, D24306, doi:10.1029/2007JD008929.

De Laat, A. T. J., et al. (2010), Validation of five years (2003–2007) of SCIAMACHY CO total column measurements using ground-based spectrometer observations, *Atmos. Meas. Tech.*, *3*, 1457–1471, doi:10.5194/amt-3-1457-2010.

Drummond, J. R., and G. S. Mand (1996), The Measurements of Pollution in the Troposphere (MOPITT) instrument: Overall performance and calibration requirements, *J. Atmos. Oceanic Technol.*, *13*, 314–320, doi:10.1175/1520-0426.

Duncan, B. N., and J. A. Logan (2008), Model analysis of the factors regulating the trends and variability of carbon monoxide between 1988 and 1997, *Atmos. Chem. Phys.*, *8*, 7389–7403.

Edwards, D. P., et al. (2006a), Satellite-observed pollution from Southern Hemisphere biomass burning, *J. Geophys. Res.*, *111*, D14312, doi:10.1029/2005JD006655.

Edwards, D. P., G. Patron, P. C. Novelli, L. K. Emmons, J. C. Gille, and J. R. Drummond (2006b), Southern Hemisphere carbon monoxide interannual variability observed by Terra/Measurement of Pollution in the Troposphere (MOPITT), *J. Geophys. Res.*, *111*, D16303, doi:10.1029/2006JD007079.

Griffith, D. W. T., N. B. Jones, and W. A. Matthews (1998), Interhemispheric ratio and annual cycle of carbonyl sulfide (OCS) total column from ground based solar FTIR spectra, *J. Geophys. Res.*, *103*(D7), 8447–8454, doi:10.1029/97JD03462.

Guenther, A., et al. (1995), A global model of natural volatile organic-compound emissions, *J. Geophys. Res.*, *100*(D5), 8873–8892, doi:10.1029/94JD02950.

Jones, N. B., C. P. Rinsland, J. B. Liley, and J. Rosen (2001), Correlation of aerosol and carbon monoxide at 45°S: Evidence of biomass burning emissions, *Geophys. Res. Lett.*, *28*(4), 709–712, doi:10.1029/2000GL012203.

Paton-Walsh, C., N. Jones, S. Wilson, A. Meier, N. Deutscher, D. Griffith, R. Mitchell, and S. Campbell (2004), Trace gas emissions from biomass burning inferred from aerosol optical depth, *Geophys. Res. Lett.*, *31*, L05116, doi:10.1029/2003GL018973.

Paton-Walsh, C., N. B. Jones, S. R. Wilson, V. Haverd, A. Meier, D. W. T. Griffith, and C. P. Rinsland (2005), Measurements of trace gas emissions from Australian forest fires and correlations with coincident measurements of aerosol optical depth, *J. Geophys. Res.*, *110*, D24305, doi:10.1029/2005JD006202.

Rinsland, C. P., et al. (1998), Northern and southern hemisphere ground-based infrared spectroscopic measurements of tropospheric carbon monoxide and ethane, *J. Geophys. Res.*, *103*(D21), 28,197–28,217, doi:10.1029/98JD02515.

Rinsland, C. P., et al. (1999), Infrared solar spectroscopic measurements of free tropospheric CO, C_2H_6, and HCN above Mauna Loa, Hawaii: Seasonal variations and evidence for enhanced emissions from the Southeast Asian tropical fires of 1997–1998, *J. Geophys. Res.*, *104*(D15), 18,667–18,680, doi:10.1029/1999JD900366.

Rinsland, C. P., N. B. Jones, B. J. Connor, S. W. Wood, A. Goldman, T. M. Stephen, F. J. Murcray, L. S. Chiou, R. Zander, and E. Mahieu (2002), Multiyear infrared solar spectroscopic measurements of HCN, CO, C_2H_6, and C_2H_2 tropospheric columns above Lauder, New Zealand (45°S latitude), *J. Geophys. Res.*, *107*(D14), 4185, doi:10.1029/2001JD001150.

Rodgers, C. D., and B. J. Connor (2003), Intercomparison of remote sounding instruments, *J. Geophys. Res.*, *108*(D3), 4116, doi:10.1029/2002JD002299.

van der Werf, G. R., J. T. Randerson, L. Giglio, G. J. Collatz, M. Mu, P. S. Kasibhatla, D. C. Morton, R. S. DeFries, Y. Jin, and T. T. van Leeuwen (2010), Global fire emissions and the contribution of deforestation, savanna, forest, agricultural, and peat fires (1997–2009), *Atmos. Chem. Phys.*, *10*, 11,707–11,735, doi:10.5194/acp-10-11707-2010.

Velazco, V., et al. (2007), Annual variation of strato-mesospheric carbon monoxide measured by ground-based Fourier transform infrared spectrometry, *Atmos. Chem. Phys.*, *7*, 1305–1312, doi:10.5194/acp-7-1305-2007.

Warner, J. X., Z. Wei, L. L. Strow, C. D. Barnet, L. C. Sparling, G. Diskin, and G. Sachse (2010), Improved agreement of AIRS tropospheric carbon monxide products with other EOS sensors using optimal estimation retrievals, *Atmos. Chem. Phys.*, *10*, 9521–9533.

Wood, S. W., et al. (2002), Validation of version 5.20 ILAS HNO_3, CH_4, N_2O, O_3 and NO_2 using ground-based measurements at Arrival Heights and Kiruna, *J. Geophys. Res.*, *107*(D24), 8208, doi:10.1029/2001JD000581.

Yashiro, H., S. Sugawara, K. Sudo, S. Aoki, and T. Nakazawa (2009), Temporal and spatial variations of carbon monoxide over the western part of the Pacific Ocean, *J. Geophys. Res.*, *114*, D08305, doi:10.1029/2008JD010876.

Zeng, G., J. A. Pyle, and P. J. Young (2008), Impact of climate change on tropospheric ozone and its global budgets, *Atmos. Chem. Phys.*, *8*(2), 369–387, doi:10.5194/acp-8-369-2008.

Zeng, G., O. Morgenstern, P. Braesicke, and J. A. Pyle (2010), Impact of stratospheric ozone recovery on tropospheric ozone and its budget, *Geophys. Res. Lett.*, *37*, L09805, doi:10.1029/2010GL042812.

Zeng, G., S. W. Wood, O. Morgenstern, N. B. Jones, J. Robinson, and D. Smale (2012), Trends, interannual and seasonal variations of tropospheric CO, C_2H_6 and HCN columns measured from ground-based FTIR at Lauder and Arrival Heights, *Atmos. Chem. Phys. Discuss.*, *12*, 6185–6204, doi:10.5194/acpd-12-6185-2012.

Zhang, X. Y. (2011), Mean global and regional distributions of MOPITT carbon monoxide during 2000–2009 and during ENSO, *Atmos. Environ.*, *45*(6), 1347–1358, doi:10.1016/j.atmosenv.2010.11.044.